Molecular Electronics

DOI: 10.1002/ange.201004055

Reticulated Heterojunctions for Photovoltaic Devices**

*Alon A. Gorodetsky, Chien-Yang Chiu, Theanne Schiros, Matteo Palma, Marshall Cox, Zhang Jia, Wesley Sattler, Ioannis Kymissis, Michael Steigerwald, and Colin Nuckolls**

Herein we present a molecular self-assembly process on the surface of transparent electrodes that yields a new type of organic semiconductor device structure: the donor deposits as supramolecular cables, and the acceptor subsequently infiltrates this network. This process results in a donor–acceptor interface that is interwoven at the nanoscale. When incorporated into photovoltaic devices, such nanostructured films provide large increases in power conversion efficiency.

To date, the most efficacious materials for organic photovoltaics are formed from the phase-segregated mixtures of semiconducting polymers and derivatized fullerenes—the bulk heterojunction (BHJ).[1–5] Phase segregation in the BHJ creates random networks of donor–acceptor domains, and these numerous domains yield an increased interfacial area, which in turn affords an increased photovoltaic response.[1–5] Efficiencies as high as 4% have been reported for single-cell BHJs with small molecules as the electron donors;[6–12] higher efficiencies have been reported for tandem cells.[13] Improving the structure and size of the donor and acceptor domains within the BHJ remains an unmet challenge.

We address this challenge with a new type of organic semiconductor, termed dibenzotetrathienocoronene (6-DBTTC; Figure 1a).[14] 6-DBTTC stacks into hole-transporting, columnar superstructures (Figure 1b), and on polymer coated indium–tin oxide (ITO) electrodes, these columns merge into a supramolecular three-dimensional network of cables. This network functions as a scaffold for the molecular recognition and directed assembly of C_{60}, thereby forming a nanostructured p–n bulk heterojunction. When incorporated into a solar cell (Figure 2a), the nanostructured active layer provides a three- to fourfold increase in the power conversion efficiency.

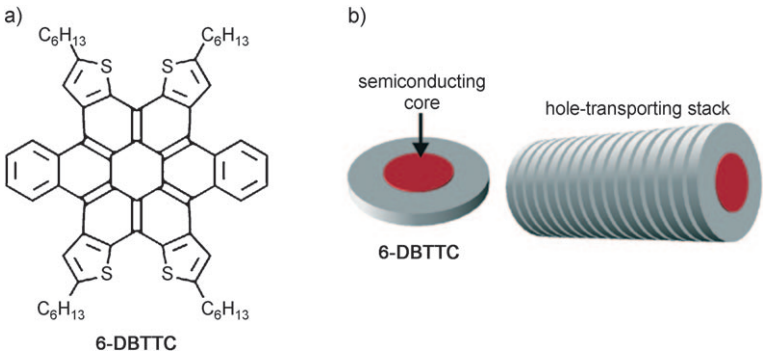

Figure 1. a) Molecular structure of 6-DBTTC. b) Illustration of the assembly of 6-DBTTC into hole-transporting columns.

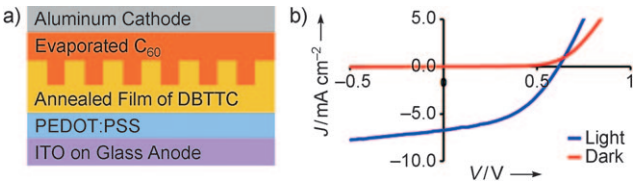

Figure 2. a) Illustration of the OPV device architecture with a nanostructured active layer. b) Typical current density–voltage (J–V) curves for a 6-DBTTC device with (blue) and without illumination (red) at 100 mW cm^{-2}.

The molecular design of 6-DBTTC incorporates two well-known organic semiconductor motifs: the contorted hexabenzocoronenes (HBCs)[15–21] and the anthradithiophenes.[8,22] Contorted HBCs consist of three fused interpenetrating pentacene subunits that form a doubly concave shape due to steric interactions at the periphery of the molecule.[15] These molecules self-organize to form columnar, hole-transporting nanostructures in liquid-crystalline phases,[15] cables,[16] and self-assembled monolayers,[17] with concomitant field effect mobilities of up to about 1 cm^2 V^{-1} s^{-1}.[23] We have

[*] Dr. A. A. Gorodetsky, C.-Y. Chiu, W. Sattler, Dr. M. Steigerwald, Prof. C. Nuckolls
Department of Chemistry and
The Center of Electron Transport in Molecular Nanostructures
Columbia University, New York, NY 10027 (USA)
Fax: (+1) 212-932-1289
E-mail: cn37@columbia.edu
Homepage: nuckolls.chem.columbia.edu
Dr. T. Schiros, M. Cox, Z. Jia, Prof. I. Kymissis
Energy Frontier Research Center
Columbia University, New York, NY 10027 (USA)
Dr. M. Palma
Department of Applied Physics and Applied Mathematics
Columbia University, New York, NY 10027 (USA)

[**] This work was supported by the Office of Naval Research under Award Numbers N00014-09-01-0250 and N00014-09-1-1117, by the National Science Foundation under Award Number CHE-0936923, and by the Center for Re-Defining Photovoltaic Efficiency Through Molecule Scale Control, an Energy Frontier Research Center funded by the U.S. Department of Energy, Office of Science, Office of Basic Energy Sciences under Award Number DE-SC0001085. The National Science Foundation (CHE-0619638) is thanked for the acquisition of an X-ray diffractometer.

Supporting information for this article is available on the WWW under http://dx.doi.org/10.1002/anie.201004055.

found that the contorted HBCs form a shape-complementary complex with n-type acceptors, such as C_{60} and C_{70}, yielding an intimate, self-assembled donor–acceptor interface.[21] In photovoltaic devices, this interface results in high open-circuit voltages and an average power conversion efficiency of about 0.55 %.[21] The present study capitalizes on the desirable properties of the HBCs and combines them with the properties of the anthradithiophene class of molecules that have been used to great effect in organic electronics.[8,22]

We have tested many HBC derivatives in OPV devices, but the 6-DBTTC is vastly superior.[24,25] The generalized architecture of the photovoltaic device is illustrated in Figure 2a. To fabricate the devices, we used clean glass substrates patterned with the ITO anode, which were in turn coated with about 40 nm of PEDOT:PSS (poly(3,4-ethylenedioxythiophene) poly(styrenesulfonate)). The 6-DBTTC was then spincast onto the PEDOT:PSS layer to a total thickness of about 90 nm (including the PEDOT:PSS layer), and the substrate was annealed at 150 °C. The active layer was completed by thermal evaporation of a circa 40 nm thick film of C_{60}. Subsequently, an aluminum cathode was deposited through a shadow mask to furnish the final device.

The current density–voltage curves exhibit almost ideal diode behavior (Figure 2b). The short-circuit current density (J_{sc}) is 6.7 mA cm^{-2}, the open-circuit voltage (V_{oc}) is 0.60 V, and the fill factor (FF) is 0.47. These parameters yield a power conversion efficiency (PCE) of about 1.9 %.[26] The corresponding external quantum efficiency (EQE) spectrum resembles both the 6-DBTTC and C_{60} thin-film spectra[27] and reaches values of $\geq$65 % (Supporting Information, Figure S1).[26] These are excellent values for small molecule BHJ organic photovoltaics.[6–12]

The 6-DBTTC molecule provides a three- to fourfold increase in efficiency compared to the HBC devices we have previously prepared.[21] We can compare the electronic properties of 6-DBTTC to HBC to help elucidate why 6-DBTTC yields more efficient devices. The 6-DBTTC highest occupied molecular orbital (HOMO) is 5.1 eV below the vacuum level and lowest unoccupied molecular orbital (LUMO) is 2.3 eV below vacuum, yielding a bandgap of 2.8 eV (Supporting Information, Figure S2).[28] These values are similar to those found for HBC,[21] and as expected 6-DBTTC acts as an electron donor. The solution absorption spectrum for 6-DBTTC is similar to that of the parent HBC (Supporting Information, Figure S3). DFT calculations reveal that the electronic structure of 6-DBTTC is dominated by the radialene-like resonance structure (Figure 1a) that characterizes the parent HBC.[18] The important conclusion is that the physical and electronic structure of 6-DBTTC closely resemble that of HBC.

The unique feature of 6-DBTTC is a heat-induced self-assembly process on the surface of the electrode (PEDOT:PSS-coated ITO). Figure 3 shows fluorescence and atomic force microscopy images of spin-cast films before and after annealing. Pristine unheated films are flat and featureless with a root-mean-square roughness of about 1 nm; few structural features are evident (Figure 3a,d). However, cable-like structures begin to emerge in films heated to 100 °C (Figure 3b,e). These structures become more numerous and

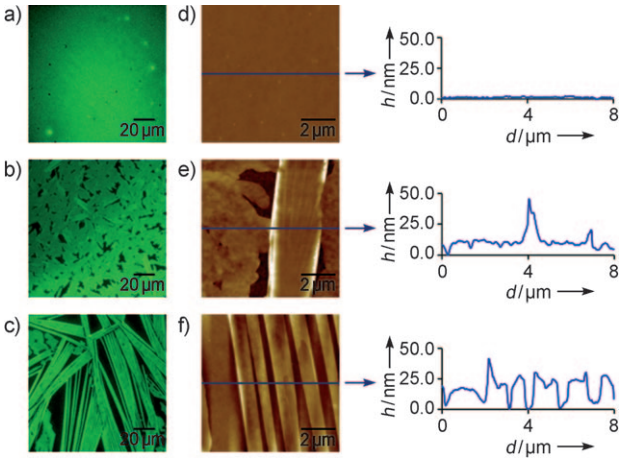

Figure 3. Fluorescence microscopy images of films from 6-DBTTC that were a) unannealed, b) annealed at 100 °C, and c) annealed at 150 °C. The corresponding noncontact AFM images and cross-sectional profiles (indicated in blue) of films from 6-DBTTC for conditions (a)–(c) are shown in (d)–(f), respectively.

pronounced for films annealed at 150 °C (Figure 3c,f), and they typically possess widths of hundreds of nanometers and heights of 10 to 30 nm. These cables are uniformly distributed over the entire electrode surface, with no apparent preferred direction of alignment. It is also important to note that the cross-sectional views of the fibers indicate that they are non-planar and possess further corrugation at the nanoscale.

To determine how important this self-assembly process is to the performance of the devices, we also tested control devices with 6-DBTTC donor layers that were either not annealed (Supporting Information, Figure S4 and S5) or were vapor-deposited rather than spin-cast (Supporting Information, Figure S6). Such devices display a drop in the current density and up to a threefold reduction in the PCE. This is similar to the efficiencies seen in the previously reported HBC-based OPV devices that do not form cables.[21]

How does 6-DBTTC pack within these cables? To answer this, we grew large ($0.43 \times 0.36 \times 0.26$ mm^3) single crystals of 6-DBTTC and measured the X-ray diffraction. Although the aromatic core could be observed, it could not be fully refined due to the low intensity (signal-to-noise ratio) of the diffraction data, thus precluding the precise determination of the atomic positions. Nevertheless, it is evident that the molecules pack in columnar stack inside a triclinic unit cell.[29]

To further elucidate the structure of the 6-DBTTC cables grown at the electrode surface, we utilized synchrotron-based grazing incidence X-ray diffraction (GIXD), as shown in Figure 4.[30] The two-dimensional pattern (Supporting Information, Figure S7) indicates strong fiber texture with diffraction intensity confined to the lateral (Q_r or in-plane) and vertical (Q_z or out-of-plane) directions, respectively, with significant differences in peak spacing along Q_r and Q_z. The Q_r pattern is dominated by the [100] and [010] reflections; a peak corresponding to diffraction from the [001] plane also appears, albeit with weaker intensity. However, the intensity ratio of these peaks is inverted in Q_z, where the [01$\bar{1}$] peak is dominant and the other reflections observed along Q_r are

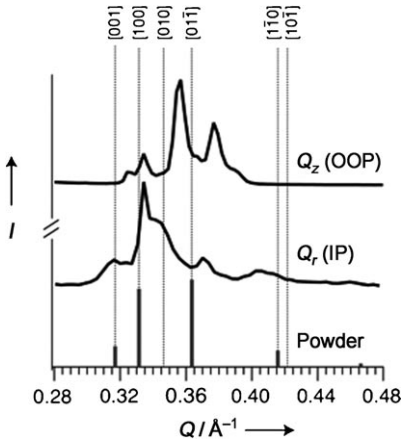

Figure 4. GIXD intensity integrated along Q_z (out-of-plane) and Q_r (in-plane) of thermally annealed (150 °C) films of 6-DBTTC on ITO. The simulated pattern based on the diffraction of the 6-DBTTC crystal is also shown.

weak or absent. The crucial point is that the peak positions of the film closely correlate to the diffraction pattern of the 6-DBTTC crystal, though the [01$\bar{1}$] peak of the film appears at a slightly lower value of Q.[31] The good agreement between the GIXD data and the simulated pattern indicates that the film is represented by pi-stacked cables, whilst the difference between in-plane and out-of-plane reflections indicates an anisotropic, three-dimensional, and crystalline network at the electrode surface.

The next step in the device preparation is the thermal evaporation of C_{60} onto these cables. The 6-DBTTC thin-film fluorescence emission is now quenched, indicating complete coverage with C_{60} (Supporting Information, Figure S8). The cables can also no longer be directly visualized by AFM and the films are relatively flat. The lack of contrast in the phase images indicates that the topmost layer consists of a single material (Supporting Information, Figure S9). Moreover, a sulfur 2p (S 2p) signal from the 6-DBTTC is observed with X-ray photoelectron spectroscopy for C_{60}-covered 6-DBTTC films[21,32,33] (Supporting Information, Figure S10). Given that the inelastic mean free path of electrons under our experimental conditions (315 eV kinetic energy) is only about 10 nm,[34] the detection of a significant number of S 2p photoelectrons supports interpenetration of the two organic layers. It is important to note that we can directly visualize the fibers beneath the C_{60} film by increasing the exposure time and gain in the fluorescence microscope (Supporting Information, Figure S8). This data in conjunction with our other physical measurements shows that we have the formation of a nanostructured active layer, in which the donor and acceptor components are interdigitated as in Figure 2a. Overall, it appears that the 6-DBBTC cables act as a template for the organization of the fullerene.

Controlled annealing of solution-processed 6-DBTTC thin films yields a crystalline donor layer, which consists of a supramolecularly assembled, three-dimensional network of cables. This network possesses a large effective interfacial surface area and further guides the subsequent assembly of fullerenes. The resulting interdigitated architecture is most likely free of the bottlenecks and dead-ends that inherently accompany typical BHJs.[2–5] Consequently, photovoltaic devices with this active layer feature high power conversion efficiencies. The simple device processing conditions also indicate that 6-DBTTC is promising partner with longer wavelength absorbers in small molecule tandem cells.[13] Furthermore, the efficiencies reported here are likely a lower limit for the potential of the 6-DBTTC motif, the UV/Vis transitions of which have a limited overlap with the solar emission spectrum.

Received: July 2, 2010
Revised: July 29, 2010
Published online: September 16, 2010

Keywords: molecular electronics · organic materials · photovoltaics · self-assembly · semiconductors

[1] M. T. Lloyd, J. E. Anthony, G. G. Malliaras, *Mater. Today* **2007**, *10*, 34.
[2] X. Yang, J. Loos, *Macromolecules* **2007**, *40*, 1353.
[3] J. Peet, M. Senatore, A. J. Heeger, G. C. Bazan, *Adv. Mater.* **2009**, *21*, 1521.
[4] G. Dennler, M. C. Scharber, C. J. Brabec, *Adv. Mater.* **2009**, *21*, 1323.
[5] A. J. Moulé, K. Meerholz, *Adv. Funct. Mater.* **2009**, *19*, 3028.
[6] L. Schmidt-Mende, A. Fechtenkötter, K. Müllen, E. Moons, R. H. Friend, J. D. MacKenzie, *Science* **2001**, *293*, 1119.
[7] F. Yang, M. Shtein, S. R. Forrest, *Nat. Mater.* **2005**, *4*, 37.
[8] M. T. Lloyd, A. C. Mayer, S. Subramanian, D. A. Mourey, D. J. Herman, A. V. Bapat, J. E. Anthony, G. G. Malliaras, *J. Am. Chem. Soc.* **2007**, *129*, 9144.
[9] B. Walker, A. B. Tamayo, X. D. Dang, P. Zalar, J. H. Seo, A. Garcia, M. Tantiwiwat, T.-Q. Nguyen, *Adv. Funct. Mater.* **2009**, *19*, 3063.
[10] U. Mayerhöffer, K. Deing, K. Grub, H. Braunschweig, K Meerholz, F. Würthner, *Angew. Chem.* **2009**, *121*, 8934; *Angew. Chem. Int. Ed.* **2009**, *48*, 8776.
[11] T. Rousseau, A. Cravino, T. Bura, G. Ulrich, R. Ziessel, J. Roncali, *Chem. Commun.* **2009**, 1673.
[12] D. Bagnis, L. Beverina, H. Huang, F. Silvestri, Y. Yao, H. Yan, G. A. Pagani, T. J. Marks, A. Facchetti, *J. Am. Chem. Soc.* **2010**, *132*, 4074.
[13] Efficiencies of about 7% have been reported for more complex tandem cell device architectures; see: T. Ameri, G. Dennler , C. Lungenschmied, C. J. Brabec, *Energy Environ. Sci.* **2009**, *2*, 347, and references therein.
[14] A detailed description of the synthesis of 6-DBTTC can be found in the Supporting Information.
[15] S. Xiao, Q. Miao, S. Sanaur, K. Pang, M. L. Steigerwald, C. Nuckolls, *Angew. Chem.* **2005**, *117*, 7556; *Angew. Chem. Int. Ed.* **2005**, *44*, 7390.
[16] S. Xiao, J. Tang, T. Beetz, X. Guo, N. Tremblay, T. Siegrist, Y. Zhu, M. Steigerwald, C. Nuckolls, *J. Am. Chem. Soc.* **2006**, *128*, 10700.
[17] X. Guo, M. Myers, S. Xiao, M. Lefenfeld, R. Steiner, G. S. Tulevski, J. Tang, J. Baumert, F. Leibfarth, J. T. Yardley, M. L. Steigerwald, P. Kim, C. Nuckolls, *Proc. Natl. Acad. Sci. USA* **2006**, *103*, 11452.
[18] Y. Cohen, S. Xiao, M. L. Steigerwald, C. Nuckolls, C. Kagan, *Nano Lett.* **2006**, *6*, 2838.
[19] X. Guo, S. Xiao, M. Myers, Q. Miao, M. L. Steigerwald, C. Nuckolls, *Proc. Natl. Acad. Sci. USA* **2009**, *106*, 691.

[20] K. N. Plunkett, K. Godula, C. Nuckolls, N. Tremblay, A. C. Whalley, S. Xiao, *Org. Lett.* **2009**, *11*, 2225.
[21] N. J. Tremblay, A. A. Gorodetsky, M. P. Cox, T. Schiros, B. Kim, R. Steiner, Z. Bullard, A. Sattler, W.-Y. So, Y. Itoh, M. F. Toney, H. Ogasawara, A. P. Ramirez, I. Kymissis, M. L. Steigerwald, C. Nuckolls, *ChemPhysChem* **2010**, *11*, 799.
[22] The incorporation of fused and pendant thiophenes in linear acenes has been shown to improve molecular stability, facilitate intermolecular π–π stacking interactions, and induce thin-film crystallinity. See: J. E. Anthony, *Chem. Rev.* **2006**, *106*, 5028 and J. E. Anthony, *Angew. Chem.* **2008**, *120*, 460; *Angew. Chem. Int. Ed.* **2008**, *47*, 452, and references therein.
[23] HBC films have shown one-dimensional photoconductivity along the aligned molecular stacks; see Refs [18] and [19].
[24] Devices with donor layers from alkyl-substituted HBC derivatives exhibited power conversion efficiencies similar to those of devices from the unsubstituted HBC in Ref. [21].
[25] See the Supporting Information and Ref. [21] for a more detailed description of the device fabrication.
[26] The external quantum efficiency and power conversion efficiency were calculated as described in: A. Moliton, J. M. Nunzi, *Polym. Int.* **2006**, *55*, 583.
[27] The thin-film 6-DBTTC spectrum is broadened and red-shifted, thereby tailing beyond 700 nm into the near infrared. Both the band broadening and red-shift are expected to aid efficient light harvesting; see Ref. [10].
[28] The corresponding HOMO and LUMO values were deduced from electrochemical studies in solution as described in: A. J. Bard, L. R. Faulkner, *Electrochemical Methods*, 2nd ed., Wiley, New York, **2001**.
[29] Unit cell: $a = 19.6$, $b = 20.2$, $c = 21.7$ Å; $\alpha = 112.4$, $\beta = 93.5$, $\gamma = 101.9°$.
[30] The GIXD patterns for 6-DBTTC on ITO and PEDOT:PSS coated ITO are very similar, with some peak broadening observed on the polymer coated surface.
[31] The critical angle for the 6-DBTTC film and ITO substrate are about 0.1° and 0.21°, respectively, so for incident angles (α) $0.1° < \alpha < 0.2°$, the X-ray light will penetrate into the film but be 100% reflected from the film-substrate interface. The intensity to the right of the $[01\bar{1}]$ peak position in Q_z is due to scattering from the $[01\bar{1}]$ peak centered around the reflected rather than the incident beam, and as such, disappears for $\alpha > 0.21°$. The offset between the "reflection-mode" $[01\bar{1}]$ peak and the primary (transmission mode) $[01\bar{1}]$ peak matches the shift with α expected from the $(2\pi/\lambda)\sin 2\theta$ relationship.
[32] G. Polzonetti, C. Battocchio, A. Goldoni, R. Larciprete, V. Carravetta, R. Paolesse, M. V. Russo, *Chem. Phys.* **2004**, *297*, 307.
[33] P. Vilmercati, C. Castellarin Cudia, R. Larciprete, C. Cepek, G. Zampieri, L. Sangaletti, S. Pagliara, A. Verdini, A. Cossaro, L. Floreano, A. Morgante, L. Petaccia, S. Lizzit, C. Battocchio, G. Polzonetti, A. Goldoni, *Surf. Sci.* **2006**, *600*, 4018.
[34] C. Martin, E. T. Arakawa, T. A. Callcott, J. C. Ashley, *J. Electron Spectrosc. Relat. Phenom.* **1985**, *35*, 307.

